Shape-Dependent Catalytic Oxidation of 2-Butanol over Pt Nanoparticles Supported on γ-Al2O3

H. Mistry,[†] F. Behafarid,[†] E. Zhou,[†] L. K. Ono,[†] L. Zhang,[‡] and B. Roldan Cuenya*[,†,§]

[†]Department of Physics, University of Central Florida, Orlando, Florida 32816, United States
[‡]Center of Functional Nanomaterials, Brookhaven National Laboratory, Upton, New York 11973-5000, United States
[§]Department of Physics, Ruhr-University Bochum, 44780 Bochum, Germany

Ⓢ Supporting Information

ABSTRACT: This study illustrates the effect of nanoparticle (NP) shape on the reactivity of size-selected Pt/γ-Al2O3 nanocatalysts for 2-butanol oxidation. Nanoparticles similar in size [transmission electron microscopy (TEM) diameter of ~1 nm] but with different shapes were prepared via encapsulation in inverse micelles. The NP shape was resolved by combining information extracted from extended X-ray absorption fine structure spectroscopy (EXAFS) data, TEM, and modeling. A correlation was observed between the average first nearest neighbor coordination number of atoms at the NP surface and their catalytic activity. In particular, the NPs with the largest number of weakly coordinated surface atoms (i.e., edges and corners) were found to be the least active for the total oxidation of 2-butanol. This result highlights that not only size but also shape control must be achieved to tailor the catalytic properties of nanoscale materials.

KEYWORDS: butanol oxidation, butanone, CO_2, Pt nanoparticle, Al_2O_3, EXAFS, shape control, size effects
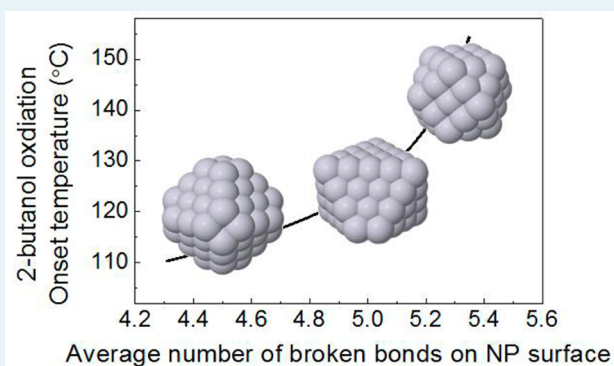
1. INTRODUCTION

The catalytic conversion of alcohols is a subject of broad interest because of the growing demand for environmentally cleaner industrial processes and fuels. Alcohols, or volatile organic compounds (VOCs), have been recognized as major components of air pollution.[1] The catalytic destruction of these compounds is a very promising approach because it requires operation temperatures much lower than those of thermal decomposition processes.[2−8] Moreover, industrially useful chemicals might be obtained through the partial oxidation of such alcohols.[9−13] For example, the partial oxidation of 2-butanol over metallic catalysts could provide a cleaner and more efficient route to the production of 2-butanone, or methyl ethyl ketone, an industrially useful solvent.[10]

Alcohols such as methanol, ethanol, and butanol are being considered as promising raw materials for hydrogen production via steam reforming or partial oxidation for use in fuel cells. Butanol may have certain advantages over methanol and ethanol because of its higher hydrogen content (higher energy density), lower vapor pressure, and lower risk of hazard generation during production.[14−16] Butanol is also emerging as an alternative to ethanol as a renewable biofuel for use in the transportation industry. Like ethanol, butanol can be produced through the fermentation of biomass. Isobutanol and 2-butanol are of special interest in gasoline blending because they can be used at concentrations in gasoline that are higher than those of ethanol.[14,17]

Because of the growing interest in butanol chemistry, understanding the parameters that influence catalytic performance in butanol reactions has become important for selectively designing more efficient catalysts. Following recent findings, parameters such as the nanoparticle (NP) structure (size and shape),[18−24] NP support,[24−28] and oxidation state of the active species[24,26,29−32] might play a role in the catalytic activity and selectivity of the supported metal NPs. Therefore, it is vital to synthesize NPs monodisperse in size, shape, and chemical composition to obtain reliable results on the respective influences of these parameters on catalytic performance.
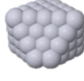
2-Butanol oxidation over metallic catalysts is interesting both as a promising means of 2-butanone production through the partial oxidation pathway and as a model for VOC elimination through total oxidation to its combustion products. The interaction of 2-butanol with metallic surfaces has been described in several studies. Yan et al.[11] reported results of the oxidation of 2-butanol on oxygen-covered Au(111) surfaces. They found that at low oxygen coverages the oxidation was highly selective toward 2-butanone and that

Table 1. Parameters Used in the Synthesis of Size- and Shape-Controlled Micellar Pt NPs[a]

Sample Name	Polymer	L	TEM diameter (nm)	Weighted TEM diameter (nm)	Model shape	Best shape N_t	Average N_s/N_t	Average Surface broken bonds
S1	PS(27700)-P2VP(4300)	0.1	1.0 ± 0.2	1.1 ± 0.2		55	0.80 ± 0.05	5.3 ± 0.2
S2	PS(16000)-P2VP(3500)	0.1	1.0 ± 0.2	1.1 ± 0.2		70	0.73 ± 0.02	5.0 ± 0.2
S3	PS(27700)-P2VP(4300)	0.2	1.0 ± 0.2	1.1 ± 0.2		79	0.70 ± 0.05	4.5 ± 0.2

[a]Molecular weight of the PS-P2VP polymers, metal salt:polymer head ratio (L), TEM diameters with error bars (standard deviation), the best model shape and the corresponding total number of atoms (N_t), and the number of surface atoms normalized by N_t (N_s/N_t). The average number of broken bonds at the NP surface obtained from the three best shapes in agreement with the EXAFS coordination numbers and TEM diameter is also shown.

when the oxygen coverage was increased both partial oxidation and complete oxidation took place simultaneously.[11] Similar results were obtained by Li et al.,[33] who described the exclusive formation of 2-butanone on oxygen-covered Pd(100) surfaces. Fewer studies are, however, available on metal NPs. Hou et al.[10] investigated the oxidation of 2-butanol over 1:3 Au:Pd NPs and found 100% selectivity for 2-butanone at ∼60 °C. The dehydrogenation of 2-butanol over Cu/SiO_2 xerogel catalysts was found to be structure-dependent by Lambert et al.[34] They observed almost no activity for highly dispersed catalysts with only a small particle size (∼3 nm), while poorly dispersed catalysts with small and large (∼15−30 nm) particles had the highest activity. For the Pt/Al_2O_3 system, the dehydration of *n*-butanol was hindered by the presence of oxygen, which promoted dehydrogenation through oxidation.[35] Pure Pt or Pt-based catalysts were found to be more active than those based on Pd,[3,36] Ru,[3,36] Rh,[3,36] Co,[3] Au,[36] Ag,[36] Ir,[36] or Ni[3] for alcohol oxidation in the liquid[36] and gas phases.[3] However, while no size dependency of the turnover frequency was detected during butanol oxidation for Pt/Al_2O_3 NP catalysts by Papaefthimiou et al.,[3] Wang et al.[36] observed the highest activities for their smallest Pt NPs (1.5−4.9 nm).

Particularly interesting is the influence of the NP shape on their reactivity.[37] For large NPs (>5 nm), this influence is mainly due to the existence of different crystalline facets associated with different NP shapes. For example, large Ag NPs (>50 nm) featuring mainly {100} facets were found to be one order of magnitude more active than truncated triangular NPs dominated by {111} facets for the oxidation of styrene.[20] However, for small NPs, the shape effect is limited not only to the specific crystallographic facets present but also to the role of highly undercoordinated atoms at corners and edges. For example, for the partial oxidation of 2-propanol to acetone, Mostafa et al.[19] found that NP shapes with a larger fraction of undercoordinated atoms at the NP surface lead to lower onset reaction temperatures, with the most active sites for that reaction being corners and edges.[19] Narayan et al.[22] also correlated the number of corner and edge atoms on a nanocatalyst surface with increased activity. Ma et al.[38] described shape effects of Pd nanocubes for the hydrogenation of 2-methyl-3-buten-2-ol and observed that {111} facets were more active than {100} facets. Effects of shape on 2-butanol oxidation, however, have not yet been described.

In this study, we investigate the oxidation of 2-butanol over Pt NP catalysts supported on γ-Al_2O_3 prepared with narrow size distributions and well-defined geometries via inverse micelle encapsulation. Transmission electron microscopy (TEM) and extended X-ray absorption fine structure spectroscopy (EXAFS) data were used to characterize the structure (size and shape) of these NP catalysts, and mass spectrometry was used to monitor their reactivity.

2. EXPERIMENTAL SECTION

a. Sample Preparation. Platinum NPs with a narrow size distribution and well-defined shapes were prepared through inverse micelle encapsulation. Toluene was used to dissolve commercially available polystyrene-block-poly(2-vinylpyridine) (PS-P2VP, Polymer Source Inc.) diblock copolymers to create reverse micelles, which were then loaded with H_2PtCl_6 to form Pt NPs. The size and shape of the NPs were controlled by varying the metal loading (metal salt:P2VP ratio) and by using polymers with different head lengths (see Table 1). Additional details about sample preparation are given in refs 18, 37, and 39. The solution was then mixed with nanocrystalline γ-Al_2O_3 powder with an ∼40 nm average grain size and stir-dried in air at ∼60 °C. The encapsulating polymer was then removed from the γ-Al_2O_3-supported Pt NPs when the sample was annealed in O_2 at 375 °C for 24 h. A 1 wt % Pt loading was used.

b. Sample Characterization. High-angle annular dark field scanning transmission electron microscopy (HAADF-STEM) images of the as-prepared samples were acquired, after the polymer had been removed, with a JEOL2001F TEM instrument operating at 200 kV. The samples were prepared for TEM by suspending the Pt/Al_2O_3 powder in methanol, placing two drops of the solution on Cu grids with holey carbon film, and drying in air. Particle diameters were determined from the TEM images by taking the full width at half maximum of the intensity profile across each particle. The TEM images were acquired after NP reduction in H_2 at 375 °C. The maximal reaction temperature was kept below the pretreatment temperature, in this case, 300 °C, to ensure lack of NP sintering.

EXAFS measurements were taken at beamline X18B of the National Synchrotron Light Source at Brookhaven National Laboratory to characterize the initial NP structure. The as-prepared Pt NP/γ-Al_2O_3 samples were first pressed into pellets and then loaded into a reaction cell. The Pt-L_3 EXAFS data

were acquired in H_2 (1:1 H_2:He ratio with a total flow rate of 25 mL/min) at room temperature after a 30 min *in situ* reduction in H_2 at 375 °C. Data processing was conducted using Athena and Artemis,[40] which are based on the IFEFFIT package.[41] Different scans were aligned to a Pt foil reference, and background was subtracted by fitting smooth curves to the pre- and post-edge data. To obtain first to fourth nearest neighbor (N_1–N_4, respectively) coordination numbers (CNs), theoretical signals were generated using the FEFF8 code[42] for a model fcc Pt structure. This theoretical model included the most important Pt–Pt scattering paths from the absorbing atom to its nearest neighbors, including multiple-scattering paths. A description of the scattering paths used can be found in refs 39, 43, and 44 along with details about the constraint of fitting parameters. R ranges of 1.9–6.0 Å and k ranges of approximately 2.5–17 Å^{-1} were used in all fits. Additional information about the fit quality parameters is given in Table S1 of the Supporting Information. As described in the Discussion, together with the TEM diameters, the EXAFS coordination numbers can be used to extract the shape of the NPs by comparison to model fcc Pt cluster structures.

Catalytic tests were conducted in a quartz packed-bed mass flow reactor. A K-type thermocouple positioned inside the bed at the catalyst level was used to monitor the temperature. Before the reaction was started, the catalysts were reduced using a 1:1 H_2/He mixture at 375 °C. The concentration of 2-butanol was controlled by passing He through a stainless steel bubbler. The reaction was conducted under oxygen-rich conditions (~20% O_2). All flows were controlled using MKS mass flow controllers. For each reaction, 50 mg of catalyst was used with a total flow rate of 50 mL/min. The concentration of reactants and products was monitored using a mass spectrometer (HPR 20 Hiden Inc.). The performance of each catalyst was studied at different temperatures ranging from 60 to 300 °C, and each test was repeated twice to ensure the reproducibility of the results.

3. RESULTS

a. Structure and Morphology. Figure 1a–c shows representative HAADF-STEM images of ligand-free Pt NP/γ-Al_2O_3 samples prepared via inverse micelle encapsulation acquired after NP reduction in H_2 at 375 °C. Histograms of the measured particle diameters for each sample show a narrow size distribution, indicating that the preparation method provides a fine degree of size control (Figure 1d–f). The average TEM diameters are listed in Table 1 together with their standard deviation.

Fourier transform EXAFS data plotted in r-space with k^2 weighting are shown in Figure 2 along with a spectrum obtained from a reference Pt foil. All measurements were taken in hydrogen after NP reduction. The corresponding k-space data, together with all r-space spectra and fits, are included in Figure S1 of the Supporting Information. In all samples studied, the NPs display a fcc structure and appear well-ordered by comparison with the bulk Pt reference (analogous features in the 4–6 Å r-space range). As described in detail in refs 39 and 43, to resolve the NP shape the spectra were fit using a multiple-scattering approach. Because of the high quality of the EXAFS data measured, information about the first to fourth nearest neighbor coordination numbers (N_1–N_4, respectively) could be extracted from the EXAFS measurements. An example of a typical EXAFS spectrum of one of our as-prepared reduced samples (S3) together with its theoretical multiple-scattering fit
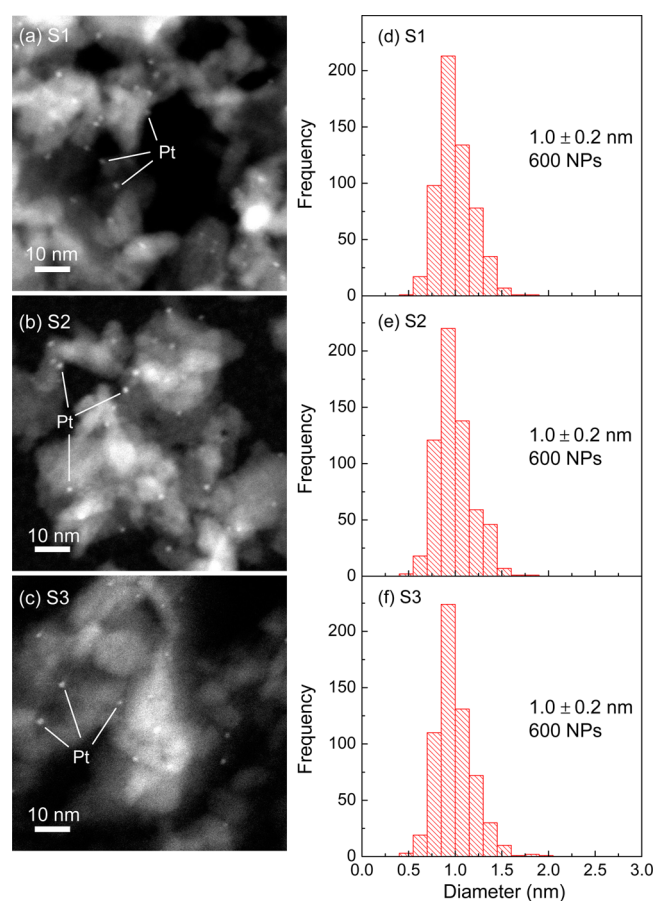

Figure 1. Representative HAADF-STEM images of Pt NPs on γ-Al_2O_3 in samples S1–S3 (a–c) acquired after removal of the encapsulating polymer and the corresponding diameter histograms (d–f).
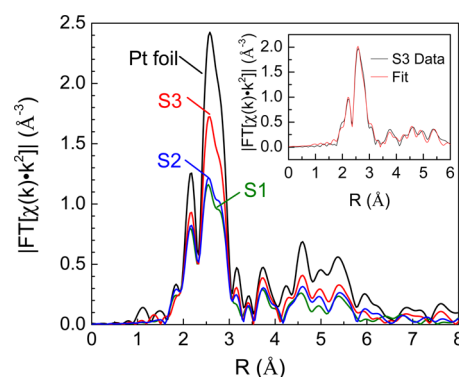

Figure 2. k^2-weighted Fourier transform EXAFS spectra of micelle-synthesized Pt NPs on γ-Al_2O_3 (samples S1–S3) and a reference Pt foil measured at room temperature in H_2 after NP reduction. The inset shows the raw data and multiscattering fit of sample S3.

is shown in the inset of Figure 2. The coordination numbers derived from this analysis for all samples are listed in Table 2. The experimentally determined coordination numbers along with the TEM diameters, taking error bars into account, were used to estimate the NP shape most prevalent in each sample by comparison with equivalent values from a database of ~4000 model fcc Pt NP shapes.[39] The three best model shapes representative of each sample were chosen by minimizing the difference between experimental and model coordination numbers and diameters. These three shapes are displayed in

Table 2. First to Fourth Nearest Neighbor Coordination Numbers (N_1–N_4) Derived from the Multiple-Scattering Analysis of EXAFS Data Acquired on As-Prepared Micelle-Synthesized Pt NPs after Reduction[a]

sample	N_1	N_2	N_3	N_4
S1	8.1 (0.7)	2.4 (1.5)	5.7 (2.5)	4.4 (1.8)
S2	8.7 (0.6)	1.7 (1.0)	5.5 (2.6)	3.3 (1.1)
S3	9.4 (0.5)	3.0 (1.4)	8.4 (2.6)	5.3 (1.6)

[a]Error bars are given in parentheses.

Table S3 of the Supporting Information, and the one providing the best agreement with the experimental parameters for each sample is included in Table 1. It should be noted that such shape determination can be reliably conducted only on narrowly distributed samples containing small NPs (<1.5 nm). For larger NPs, there would be a much larger degeneracy of shapes that would fit the same set of experimental coordination numbers for a given TEM NP diameter.

b. Catalytic Reactivity. Figure 3 shows the conversion of 2-butanol over each Pt NP/Al$_2$O$_3$ sample under oxidation at
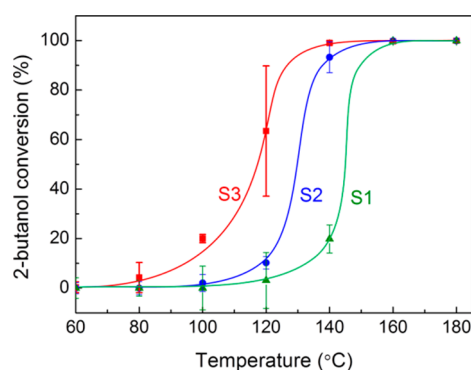
Figure 3. Catalytic performance of micelle-synthesized Pt NPs during the oxidation of 2-butanol measured at different temperatures under steady-state reaction conditions. Each experiment was repeated at least twice on fresh samples from the same catalyst batch. Error bars indicate maximal and minimal conversions measured at each temperature from two reproducibility experiments. Solid lines are guides for the eye.

different temperatures. Data at each temperature were taken under steady-state reaction conditions. In general, the oxidation of 2-butanol started at ~100 °C, and maximal conversion was reached at ~160 °C for all the catalysts studied. The reactivity of the Al$_2$O$_3$ support alone for 2-butanol oxidation was also measured at different temperatures, and a maximal conversion of 10% was found to occur below 180 °C, indicating that the Al$_2$O$_3$ powder makes an insignificant contribution to the conversion measured for each sample.

The reaction products detected for the oxidation of 2-butanol were 2-butanone, carbon dioxide, and water. At low temperatures (<140–160 °C, depending on the NP shape), while the overall conversion is low, the reaction is more selective toward partial oxidation of 2-butanol, producing 2-butanone and water, as expected following reaction pathway 1:

$$C_4H_{10}O + \frac{1}{2}O_2 \rightarrow C_4H_8O + H_2O \tag{1}$$
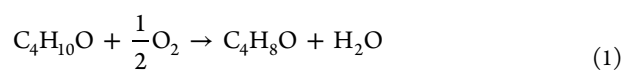
At higher temperatures (>160–200 °C), 2-butanol undergoes complete oxidation to carbon dioxide and water, described by reaction pathway 2:

$$C_4H_{10}O + 6O_2 \rightarrow 4CO_2 + 5H_2O \tag{2}$$
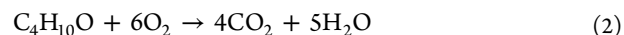
The total conversion together with the selectivity toward each reaction pathway at each temperature is shown in Figure 4. From 25 to 120 °C, the total conversion is low; however, the
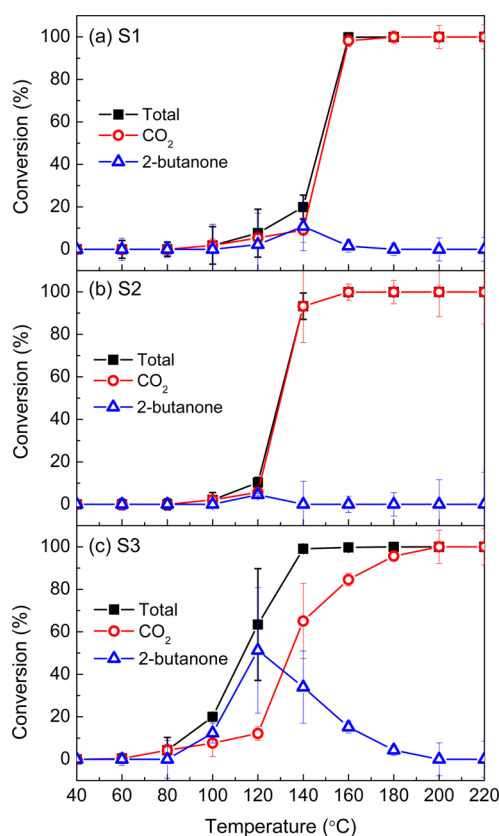
Figure 4. Total 2-butanol conversion (■), conversion of 2-butanol to 2-butanone (△), and conversion of 2-butanol to carbon dioxide (○) during the oxidation of 2-butanol over micelle-synthesized Pt NPs/γ-Al$_2$O$_3$ for samples S1–S3 (a–c, respectively). Error bars indicate maximal and minimal conversions measured at each temperature in reproducibility experiments under identical reaction conditions.

conversion toward the formation of 2-butanone is favored over the production of CO$_2$ in all samples. At 120 °C, the selectivity for 2-butanone begins to decrease, while the selectivity toward CO$_2$ increases. Complete oxidation of 2-butanol to CO$_2$ is achieved with 100% selectivity at approximately 160 °C for S1, 140 °C for S2, and 200 °C for S3.

4. DISCUSSION

The NP samples in this study were prepared using colloidal chemistry by loading inverse micelles formed from PS-2VP diblock copolymers with different molecular weights and distinct metal:P2VP ratios with a Pt salt (see Table 1). Because of the very small size of the NPs (~1 nm) and the high absorption of the thicker nanocrystalline Al$_2$O$_3$ support, HAADF-STEM measurements were used to obtain adequate contrast between the NPs and the support. Under these conditions, only the diameter of the NPs could be resolved, not their shape. Although TEM measurements provide similar

average NP diameters with narrow size distributions for all samples, distinct catalytic behavior is observed (Figure 3), in particular, a different onset reaction temperature (Figures 3 and 5), distinct selectivity at a given temperature (S1 and S2
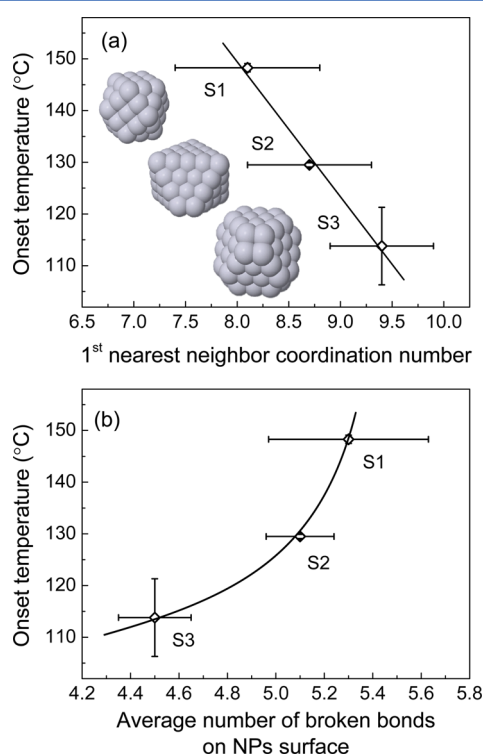

Figure 5. Onset reaction temperature (temperature of 50% conversion) as a function of (a) first nearest neighbor coordination number (EXAFS) and (b) the average number of missing bonds on the NP surface.

compared to S3), and a different transition temperature from the partial (2-butanone as the main product) to the total oxidation of 2-butanol (CO_2 as the product) (S1 and S2 compared to S3) (Figure 4).

It should be noted that the morphological characterization of our NPs, revealing small size-selected NPs, was performed after pretreatment in H_2 at 375 °C, but before exposure to the reactant. Nevertheless, because the reaction temperature never exceeded 300 °C, NP stability against sintering is expected. In fact, previous work by our group on micellar Pt/Al_2O_3 NPs showed that the EXAFS spectra and TEM images of the as-prepared H_2-pretreated NPs were analogous to those measured after the 2-propanol oxidation reaction at similar temperatures after subsequent reduction in hydrogen, corroborating the absence of coarsening.[45] The NPs used in this study were exposed to comparable oxygen-rich conditions and had reached 100% conversion of 2-butanol at 240 °C, so it is unlikely that NP sintering occurred. In addition, the thermal stability of identical micellar Pt/Al_2O_3 NPs up to 450 °C in O_2 was previously demonstrated.[46]

To understand the structure−reactivity trends observed for nearly identically sized NPs, the TEM diameters and EXAFS coordination numbers were used to obtain a model for the dominant NP shape in each sample. As shown in Table 2, the EXAFS coordination numbers of samples S1−S3 are different, indicating the presence of NPs with distinct shapes. For example, for a given TEM NP diameter, flatter NPs are

characterized by lower average coordination numbers. According to the first NN CNs listed in Table 2, sample S1 has the lowest value of N_1 and S3 the highest. Therefore, S1 should have the smallest and/or the flattest NPs and S3 the largest and/or the most three-dimensional NPs. As described in more detail in refs 39 and 43 and the Supporting Information, via determination of the shape of the NPs, other useful parameters such as the total number of atoms (N_t), the ratio of the atoms at the NP surface normalized by the total number of atoms (N_s/N_t), and the average number of broken bonds at the NP surface can be obtained. A Pt atom in a bulk fcc structure has a first NN CN of 12, but surface atoms on NPs have lower CNs depending on their specific location. The number of broken bonds for each surface atom is defined as $12 − N_1$ of that atom. While N_s/N_t represents the surface:bulk ratio, which is expected to be larger for smaller NPs, the average number of missing bonds depends mainly on the distinct NP facets and also the number of atoms at corner and edge sites. For instance, Pt(111) and Pt(100) facets have average numbers of missing bonds of three and four, respectively, while this value could be higher (up to eight) for atoms at NP corners and edges.

Figure 5a shows a clear correlation between the onset reaction temperature (T of 50% conversion) and the first NN CN (N_1) obtained from the EXAFS analysis of Figure 3. Interestingly, samples with lower coordination numbers (smaller and/or flatter) have higher onset reaction temperatures and lower activities for 2-butanol oxidation. A similar trend is observed in Figure 5b, where the onset reaction temperature is higher for the samples with the largest number of atoms at corner and edge sites, namely, those with the largest number of broken bonds at the NP surface. This is contrary to our previous findings for 2-propanol partial oxidation, where it was shown that the NPs with the largest number of broken bonds were the most active.[19] To understand the difference between these two studies, we should take into account the selectivity of our catalysts in the 2-propanol and 2-butanol oxidation reactions. In the case of 2-propanol, the onset temperature for its partial oxidation to acetone ranges from 45 to 85 °C, depending on the specific NP shape, with more than 90% selectivity toward partial oxidation for all samples investigated below 100 °C. In a follow-up study, *operando* EXAFS and X-ray absorption near edge spectroscopy (XANES) data revealed a correlation between the chemical state of ∼0.7 nm Pt NPs and the switch in the selectivity observed from the partial (acetone) to total oxidation (CO_2) of 2-propanol above ∼140 °C.[45] Specifically, it was demonstrated that the partial oxidation of 2-propanol occurs when the NPs are oxidized (<140 °C), while the total oxidation pathway becomes dominant over metallic Pt NPs with a surface covered by chemisorbed oxygen (>140 °C).[45] In contrast, in the case of 2-butanol, conversion toward the partial oxidation product 2-butanone is low at all temperatures (nearly negligible for S1 and S2 and only clearly detectable for S3 below 160 °C), and the temperature required to achieve 100% total conversion is higher (140−160 °C), but also dependent on the specific NP geometric structure. In addition, in this case, 100% conversion of 2-butanol is never achieved during its partial oxidation temperature regime, only at high temperature during its total oxidation to CO_2.

The trend previously observed for 2-propanol partial oxidation[19] (undercoordinated Pt atoms more active) is the opposite of the trend obtained here for 2-butanol total oxidation. A possible explanation for the shape dependency

observed here could be the size-dependent stability of Pt oxide species. Binding of oxygen to Pt is stronger for smaller NPs,[47−49] and therefore, Pt oxide decomposition is expected to require a higher temperature on smaller NPs. Assuming that metallic Pt is the active species for the total oxidation of butanol to CO_2 (similar to 2-propanol),[45] the higher onset temperature for 2-butanol oxidation over smaller NPs could be due to the higher temperature needed for Pt oxide decomposition. Similar structure-dependent reactivity trends have been shown in the literature for complete oxidation of various hydrocarbons over Pt/Al$_2$O$_3$ catalysts, with larger NPs showing higher activity because of their lower susceptibility to oxide formation.[50−53] Carlsson et al.[52] prepared Pt/Al$_2$O$_3$ monolith catalysts with particle sizes ranging from 10 to 48 nm for the total oxidation of propane at varying oxygen concentrations, and their experiments showed a decrease in activity after exposure to oxygen-rich conditions, most likely because of oxide formation. Furthermore, catalysts with large Pt NPs showed higher activity and could withstand higher oxygen concentrations before experiencing a decrease in activity as compared to smaller Pt NPs, indicating that the larger NPs are more difficult to oxidize than the smaller NPs. Also, for the oxidation of propane, Yazawa et al.[53] found higher turnover frequencies (TOFs) for Pt/Al$_2$O$_3$ catalysts with lower dispersion, resulting from the lower degree of oxidation of larger Pt NPs as revealed by XANES.

In addition to the PtOx decomposition effect, the binding energy of chemisorbed oxygen species that might be present under reaction conditions at higher temperatures could also play a role in the shape-dependent reactivity obtained. Papaefthimiou et al.[3] studied the oxidation of benzene, butanol, and ethyl acetate over Pt/Al$_2$O$_3$ catalysts and fit their reaction data using a simple power law rate equation. Remarkably, the highest reaction order with respect to VOC concentration was found for the butanol oxidation reaction, where the most negative reaction order for oxygen was obtained. Such a negative reaction order was interpreted as the inhibition effect of oxygen, suggesting a Langmuir−Hinshelwood type of reaction mechanism. Along this line, the expected higher binding energy of chemisorbed oxygen on smaller NPs[47,48] or NP shapes with a larger fraction of strong binding sites (corners and edges) would lower the reaction rate and increase the onset temperature, which was observed in our study. Similar results showing higher activity for larger NP sizes have been obtained for the complete oxidation of other VOCs over the Pt/Al$_2$O$_3$ system.[54−61] For example, Radic et al.[54] compared 1.0 and 15.5 nm Pt/Al$_2$O$_3$ NPs in the complete oxidation of n-hexane and toluene, finding TOFs 10 times higher for the larger particles than the smaller for both alcohols because of the decreased Pt−O bond strength in the larger particles.

In summary, a shape-dependent trend was observed for the onset reaction temperature during the oxidation of 2-butanol, where NPs with the smallest number of weakly coordinated atoms (smallest number of broken bonds) at the NP surface displayed the best catalytic performance at low temperatures. The total oxidation of 2-butanol to CO_2 was the dominant reaction pathway, and metallic Pt surfaces decorated by chemisorbed oxygen were found to be the active species during this reaction. Therefore, the shape-dependent reactivity can be explained by a lower PtO$_x$ decomposition temperature and weaker binding of chemisorbed oxygen on NPs with less broken bonds at the surface, which favors the total oxidation pathway.

Our study illustrates the critical role played by the NP structure, specifically its size and shape, in its catalytic performance, in particular, the onset reaction temperature, preferred reaction pathway, and selectivity.

5. CONCLUSIONS

Small (∼1 nm) size- and shape-controlled Pt NPs supported on γ-Al$_2$O$_3$ were used as a model system to investigate structure−reactivity relationships during the oxidation of 2-butanol. A shape dependency of the onset reaction temperature was observed, with decreasing activity detected for NPs with the largest number of undercoordinated surface atoms. In addition, very low activity for the partial oxidation of 2-butanol was obtained, with only a low conversion to 2-butanone observed for S3 below 160 °C. The dominant reaction pathway toward CO_2 formation was favored by the presence of Pt NPs with a small number of edge and corner sites. This result is explained considering the negative effect that the strong binding of oxygen to such sites (through the stabilization of chemisorbed oxygen or that of PtO$_x$ species) might have on the total oxidation pathway.

Our study emphasizes the importance of tailoring the structure of catalysts at the atomic level to gain control of not only their catalytic activity but also their selectivity and optimal operation temperature.

■ ASSOCIATED CONTENT

Ⓢ Supporting Information
Details of the EXAFS multiscattering analysis, including fit parameters, fit quality factors, and plots of measured data and fits (Tables S1 and S2 and Figure S1), and a description of NP shape modeling with a table showing the best model shapes representative of each sample (Table S3). This material is available free of charge via the Internet at http://pubs.acs.org.

■ AUTHOR INFORMATION

Corresponding Author
*E-mail: beatriz.roldan@rub.de.
Notes
The authors declare no competing financial interest.

■ ACKNOWLEDGMENTS

■ REFERENCES

(1) Azalim, S.; Franco, M.; Brahmi, R.; Giraudon, J. M.; Lamonier, J. F. *J. Hazard. Mater.* **2011**, *188*, 422−427.
(2) Spivey, J. J. *Ind. Eng. Chem. Res.* **1987**, *26*, 2165−2180.

(3) Papaefthimiou, P.; Ioannides, T.; Verykios, X. E. *Appl. Catal., B* **1997**, *13*, 175−184.

(4) Hermia, J.; Vigneron, S. *Catal. Today* **1993**, *17*, 349−358.

(5) Everaert, K. *J. Hazard. Mater.* **2004**, *109*, 113−139.

(6) Papaefthimiou, P.; Ioannides, T.; Verykios, X. E. *Appl. Therm. Eng.* **1998**, *18*, 1005−1012.

(7) Abbasi, Z.; Haghighi, M.; Fatehifar, E.; Saedy, S. *J. Hazard. Mater.* **2011**, *186*, 1445−1454.

(8) Takamitsu, Y.; Yoshida, S.; Kobayashi, W.; Ogawa, H.; Sano, T. *J. Environ. Sci. Health, Part A: Toxic/Hazard. Subst. Environ. Eng.* **2013**, *48*, 667−674.

(9) Wang, Z.; Ma, H.; Zhu, W.; Wang, G. *React. Kinet. Catal. Lett.* **2002**, *76*, 271−279.

(10) Hou, W. B.; Dehm, N. A.; Scott, R. W. J. *J. Catal.* **2008**, *253*, 22−27.

(11) Yan, T.; Gong, J.; Mullins, C. B. *J. Am. Chem. Soc.* **2009**, *131*, 16189−16194.

(12) Fang, D. R.; Ren, W. Z.; Liu, Z. M.; Xu, X. F.; Xu, L.; Lu, H. Y.; Liao, W. P.; Zhang, H. M. *J. Nat. Gas Chem.* **2009**, *18*, 179−182.

(13) Vinod, C. P.; Wilson, K.; Lee, A. F. *J. Chem. Technol. Biotechnol.* **2011**, *86*, 161−171.

(14) Nahar, G. A.; Madhani, S. S. *Int. J. Hydrogen Energy* **2010**, *35*, 98−109.

(15) Wang, W.; Cao, Y. *Int. J. Hydrogen Energy* **2011**, *36*, 2887−2895.

(16) Wang, W. J.; Cao, Y. Y. *Int. J. Hydrogen Energy* **2010**, *35*, 13280−13289.

(17) Dagaut, P.; Sarathy, S. M.; Thomson, M. J. *Proc. Combust. Inst.* **2009**, *32*, 229−237.

(18) Croy, J. R.; Mostafa, S.; Liu, J.; Sohn, Y. H.; Roldan Cuenya, B. *Catal. Lett.* **2007**, *118*, 1−7.

(19) Mostafa, S.; Behafarid, F.; Croy, J. R.; Ono, L. K.; Li, L.; Yang, J. C.; Frenkel, A. I.; Roldan Cuenya, B. *J. Am. Chem. Soc.* **2010**, *132*, 15714−15719.

(20) Xu, R.; Wang, D. S.; Zhang, J. T.; Li, Y. D. *Chem.—Asian J.* **2006**, *1*, 888−893.

(21) Bratlie, K. M.; Lee, H.; Komvopoulos, K.; Yang, P.; Somorjai, G. A. *Nano Lett.* **2007**, *7*, 3097−3101.

(22) Narayanan, R.; El-Sayed, M. A. *J. Phys. Chem. B* **2005**, *109*, 12663−12676.

(23) Zaera, F. *J. Phys. Chem. Lett.* **2010**, *1*, 621−627.

(24) Roldan Cuenya, B. *Thin Solid Films* **2010**, *518*, 3127−3150.

(25) Croy, J. R.; Mostafa, S.; Liu, J.; Sohn, Y. H.; Heinrich, H.; Roldan Cuenya, B. *Catal. Lett.* **2007**, *119*, 209−216.

(26) Comotti, M.; Li, W.-C.; Spliethoff, B.; Schüth, F. *J. Am. Chem. Soc.* **2006**, *128*, 917−924.

(27) Sathish, M.; Viswanath, R. *Catal. Today* **2007**, *129*, 421−427.

(28) Bonanni, S.; Aït-Mansour, K.; Harbich, W.; Brune, H. *J. Am. Chem. Soc.* **2012**, *134*, 3445−3450.

(29) Singh, J.; Alayon, E. M. C.; Tromp, M.; Safonova, O. V.; Glatzel, P.; Nachtegaal, M.; Frahm, R.; van Bokhoven, J. A. *Angew. Chem., Int. Ed.* **2008**, *47*, 9260−9264.

(30) Ackermann, M. D.; Pedersen, T. M.; Hendriksen, B. L.; Robach, O.; Bobaru, S. C.; Popa, I.; Quiros, C.; Kim, H.; Hammer, B.; Ferrer, S.; Frenken, J. W. *Phys. Rev. Lett.* **2005**, *95*, 255505.

(31) Balint, I.; Miyazaki, A.; Aika, K. *J. Catal.* **2003**, *220*, 74−83.

(32) Merte, L. R.; Ahmadi, M.; Behafarid, F.; Ono, L. K.; Lira, E.; Matos, J.; Li, L.; Yang, J. C.; Roldan Cuenya, B. *ACS Catal.* **2013**, *3*, 1460−1468.

(33) Li, Z.; Tysoe, W. T. *Surf. Sci.* **2010**, *604*, 1377−1387.

(34) Lambert, S.; Cellier, C.; Ferauche, F.; Gaigneaux, É. M.; Heinrichs, B. *Catal. Commun.* **2007**, *8*, 2032−2036.

(35) Sedjame, H. J.; Lafaye, G.; Barbier, J. *Appl. Catal., B* **2013**, *132−133*, 132−141.

(36) Wang, T.; Shou, H.; Kou, Y.; Liu, H. C. *Green Chem.* **2009**, *11*, 562−568.

(37) Roldan Cuenya, B. *Acc. Chem. Res.* **2013**, *46*, 1682−1691.

(38) Ma, R.; Semagina, N. *J. Phys. Chem. C* **2010**, *114*, 15417−15423.

(39) Roldan Cuenya, B.; Croy, J. R.; Mostafa, S.; Behafarid, F.; Li, L.; Zhang, Z.; Yang, J. C.; Wang, Q.; Frenkel, A. I. *J. Am. Chem. Soc.* **2010**, *132*, 8747−8756.

(40) Ravel, B.; Newville, M. *J. Synchrotron Radiat.* **2005**, *12*, 537−541.

(41) Newville, M. *J. Synchrotron Radiat.* **2001**, *8*, 322−324.

(42) Ankudinov, A. L.; Bouldin, C. E.; Rehr, J. J.; Sims, J.; Hung, H. *Phys. Rev. B* **2002**, *65*, 104107.

(43) Roldan Cuenya, B.; Frenkel, A. I.; Mostafa, S.; Behafarid, F.; Croy, J. R.; Ono, L. K.; Wang, Q. *Phys. Rev. B* **2010**, *82*, 155450.

(44) Frenkel, A. I.; Hills, C. W.; Nuzzo, R. G. *J. Phys. Chem. B* **2001**, *105*, 12689−12703.

(45) Paredis, K.; Ono, L. K.; Mostafa, S.; Li, L.; Zhang, Z.; Yang, J. C.; Barrio, L.; Frenkel, A. I.; Roldan Cuenya, B. *J. Am. Chem. Soc.* **2011**, *133*, 6728−6735.

(46) Matos, J.; Ono, L.; Behafarid, F.; Croy, J.; Mostafa, S.; DeLaRiva, A.; Datye, A.; Frenkel, A.; Cuenya, B. R. *Phys. Chem. Chem. Phys.* **2012**, *14*, 11457−11467.

(47) Xu, Y.; Shelton, W. A.; Schneider, W. F. *J. Phys. Chem. B* **2006**, *110*, 16591−16599.

(48) Ono, L. K.; Croy, J. R.; Heinrich, H.; Roldan Cuenya, B. *J. Phys. Chem. C* **2011**, *115*, 16856−16866.

(49) Wang, C.-B.; Yeh, C.-T. *J. Catal.* **1998**, *178*, 450−456.

(50) Arnby, K.; Assiks, J.; Carlsson, P.-A.; Palmqvist, A.; Skoglundh, M. *J. Catal.* **2005**, *233*, 176−185.

(51) Völter, J.; Lietz, G.; Spindler, H.; Lieske, H. *J. Catal.* **1987**, *104*, 375−380.

(52) Carlsson, P.-A.; Mollner, S.; Arnby, K.; Skoglundh, M. *Chem. Eng. Sci.* **2004**, *59*, 4313−4323.

(53) Yazawa, Y.; Yoshida, H.; Hattori, T. *Appl. Catal., A* **2002**, *237*, 139−148.

(54) Radic, N.; Grbic, B.; Terlecki-Baricevic, A. *Appl. Catal., B* **2004**, *50*, 153−159.

(55) Garetto, T.; Apesteguıa, C. *Catal. Today* **2000**, *62*, 189−199.

(56) Garetto, T.; Apesteguıa, C. *Appl. Catal., B* **2001**, *32*, 83−94.

(57) Otto, K.; Andino, J.; Parks, C. *J. Catal.* **1991**, *131*, 243−251.

(58) Gololobov, A. M.; Bekk, I. E.; Bragina, G. O.; Zaikovskii, V. I.; Ayupov, A. B.; Telegina, N. S.; Bukhtiyarov, V. I.; Stakheev, A. Y. *Kinet. Catal.* **2009**, *50*, 830−836.

(59) Briot, P.; Auroux, A.; Jones, D.; Primet, M. *Appl. Catal.* **1990**, *59*, 141−152.

(60) Carballo, L. M.; Wolf, E. E. *J. Catal.* **1978**, *53*, 366−373.

(61) Yang, J.; Tschamber, V.; Habermacher, D.; Garin, F.; Gilot, P. *Appl. Catal., B* **2008**, *83*, 229−239.